



UvA-DARE (Digital Academic Repository)

A liquid-liquid transition in supercooled aqueous solution related to the HDA-LDA transition

Woutersen, S.; Ensing, B.; Hilbers, M.; Zhao, Z.; Angell, C.A.

DOI

[10.1126/science.aao7049](https://doi.org/10.1126/science.aao7049)

Publication date

2018

Document Version

Final published version

Published in

Science

License

Article 25fa Dutch Copyright Act (<https://www.openaccess.nl/en/policies/open-access-in-dutch-copyright-law-taverne-amendment>)

[Link to publication](#)

Citation for published version (APA):

Woutersen, S., Ensing, B., Hilbers, M., Zhao, Z., & Angell, C. A. (2018). A liquid-liquid transition in supercooled aqueous solution related to the HDA-LDA transition. *Science*, 359(6380), 1127-1131. <https://doi.org/10.1126/science.aao7049>

General rights

It is not permitted to download or to forward/distribute the text or part of it without the consent of the author(s) and/or copyright holder(s), other than for strictly personal, individual use, unless the work is under an open content license (like Creative Commons).

Disclaimer/Complaints regulations

If you believe that digital publication of certain material infringes any of your rights or (privacy) interests, please let the Library know, stating your reasons. In case of a legitimate complaint, the Library will make the material inaccessible and/or remove it from the website. Please Ask the Library: <https://uba.uva.nl/en/contact>, or a letter to: Library of the University of Amsterdam, Secretariat, P.O. Box 19185, 1000 GD Amsterdam, The Netherlands. You will be contacted as soon as possible.

UvA-DARE is a service provided by the library of the University of Amsterdam (<https://dare.uva.nl>)

WATER STRUCTURE

A liquid-liquid transition in supercooled aqueous solution related to the HDA-LDA transition

Sander Woutersen,^{1*} Bernd Ensing,^{1,2} Michiel Hilbers,¹ Zuofeng Zhao,³ C. Austen Angell^{3*}

Simulations and theory suggest that the thermodynamic anomalies of water may be related to a phase transition between two supercooled liquid states, but so far this phase transition has not been observed experimentally because of preemptive ice crystallization. We used calorimetry, infrared spectroscopy, and molecular dynamics simulations to investigate a water-rich hydrazinium trifluoroacetate solution in which the local hydrogen bond structure surrounding a water molecule resembles that in neat water at elevated pressure, but which does not crystallize upon cooling. Instead, this solution underwent a sharp, reversible phase transition between two homogeneous liquid states. The hydrogen-bond structures of these two states are similar to those established for high- and low-density amorphous (HDA and LDA) water. Such structural similarity supports theories that predict a similar sharp transition in pure water under pressure if ice crystallization could be suppressed.

The divergent behavior of pure-water thermodynamic properties during deep supercooling was interpreted by Poole *et al.* (1) in terms of the existence of a nearby second critical point at which two liquid phases, differing in density, become identical. A thermodynamic model, a variant of the van der Waals equation of state, was devised by Poole *et al.* (2), to show how the two critical points could be related through the splitting of the familiar van der Waals coexistence domain into two segments. Poole *et al.* (2) argued that this splitting would result if a liquid structure of low coordination number could be stabilized, by directional bonding, at a density that is intermediate between gas and close-packed liquid, as occurs in ice and in random tetrahedral network models of water (3).

However, for studies of pure water in the laboratory, none of this latter scenario can be established by direct experimentation because of the preempting crystallization of ice I_h (ordinary ice) that forms by homogeneous nucleation and growth in a pattern that closely follows the pattern of divergences of the thermodynamic susceptibilities (4). The addition of second components (salts or other liquids) can depress crystallization rates (i.e., act as antifreeze) and permit formation of glassy phases. This approach can act as a proxy for pressure increases for mapping out the phase diagram. Theory (5–7) indicates the possibility of obtaining information on hidden critical phenomena in single-component systems by virtue of critical lines emanating from the pure solvent

into the binary solution. Unfortunately, most ionic (8–10) and many molecular (11) second components destroy the water anomalies more rapidly than they block the nucleation of ice.

Recently, however, a class of ionic solutes has been discovered for which the latter discouraging scenario is reversed; that is, they permit supercooling to the point of vitrification without destruction of the liquid-state anomalies. Rather, they seem to displace the second critical point to lower pressures and temperatures, as described by Anisimov and colleagues (6, 7), in such a way that the ambient-temperature cooling leads the system to cross a liquid-liquid coexistence line before any ice crystallization can occur (12). Thus, the “crystallization curtain” can be lifted.

The solutions in which these observations have been made obey the ideal-solution laws for depression of the ice melting point (12, 13). Such behavior indicates that the solute ion–water

molecule and water molecule–water molecule interactions are not distinguishable from the point of view of thermodynamics, so that thermodynamically the water molecules will continue to behave in waterlike ways, one of which is to undergo a phase transition in the absence of ice crystallization. Although we investigate ideal solutions here, we note that the arguments of Anisimov (6) and of Biddle *et al.* (7) for the displacement of the critical point to lower temperatures and pressures also hold in nonideal solutions and are consistent with computer simulation findings for NaCl–water solutions (14, 15).

Figure 1 shows the thermodynamic behavior that is revealed when cooling an ideal aqueous solution. Instead of salt addition leading to a replacement of the pure water anomaly with a decreasing solution molar heat capacity (C_p) and finally a glass transition [as shown for the familiar case of an 11.4 mole percent (mol %) LiCl solution (9)], we saw an almost first-order–like spike in heat capacity in the case of solutions of ionic liquid hydrazinium trifluoroacetate (N_2H_5TFA), although the salt content was higher for the latter case. The “spike anomaly” was fully reversible upon reheating; it was followed, at higher temperature, by crystallization of ice I_h . In (12), it was noted that the onset of the heat capacity anomaly was preceded by a density anomaly—a flattening out of the density decrease with decreasing temperature. Against the background of linearly decreasing density with decreasing T , the flattening corresponds to an anomalous density decrease approaching the C_p maximum. Unfortunately, at the highest water content, 84.4 mol %, where the sharp transition of the present work occurs, the density anomaly could not be observed. The reasons are straightforwardly related to the sample size required for the density measurement (16).

A related phenomenon has been reported by Murata and Tanaka (17) using glycerol as the solute, but in that case, the formation of the second liquid phase was accompanied by ice formation and so was irreversible. The problem then becomes one of identifying the participating structures in the new, almost first-order transition.

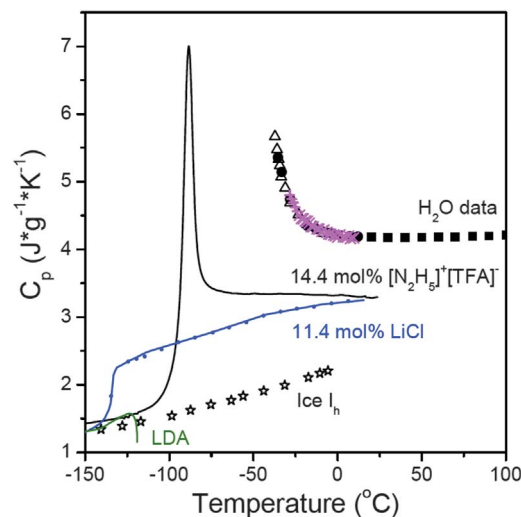


Fig. 1. Contrasting thermal behavior of ideal and nonideal aqueous solutions during supercooling. Com-

positions are identified on the plots. Apparent values of C_p were determined during cooling scans at 20 K min^{-1} in each case. Data for pure H_2O are a compendium of reported results [see (12)]. Data for the LiCl solution are from (9).

¹Van 't Hoff Institute for Molecular Sciences, University of Amsterdam, Science Park 904, 1098 XH Amsterdam, Netherlands.

²Catalan Institute of Nanoscience and Nanotechnology (ICN2), CSIC and Barcelona Institute of Science and Technology, Campus UAB, Bellaterra, 08193 Barcelona, Spain. ³School of Molecular Sciences, Arizona State University, Tempe, AZ 85287, USA.

*Corresponding author. Email: s.woutersen@uva.nl (S.W.); austenangell@gmail.com (C.A.A.)

As a probe, the decoupled vibration frequency of the OH oscillator is ideal because its frequency is very sensitive to the OH...O H-bond strength.

We prepared aqueous solutions of N_2H_5TFA with molar water fractions x_{water} ranging from 0.50 to 0.84 (16). The small sample volume ($\sim 1 \mu L$), kept between two CaF_2 windows separated by $\sim 25 \mu m$; Fig. 2A) allowed for comparatively slow temperature scans without crystallization. Water volumes of this size ($>10^{19}$ molecules) behave thermodynamically like bulk water (16). We used dilute H/D isotopic mixtures (H:D fraction ~ 0.03) to prevent coupling between the OH-stretch modes (18). This choice ensured that the center frequency and width of the OH-stretch absorption peak reflected the H-bond structure. The thermodynamics of H_2O and D_2O are essentially the same, once a correction for the zero-point motion is taken into account (19, 20). Figure 2B shows the infrared (IR) absorption spectrum of an $x_{water} = 0.84$ solution at room temperature (red curve) and down to 140 K during cooling at $7 K min^{-1}$ (spectra are shown at 2.2 K temperature intervals).

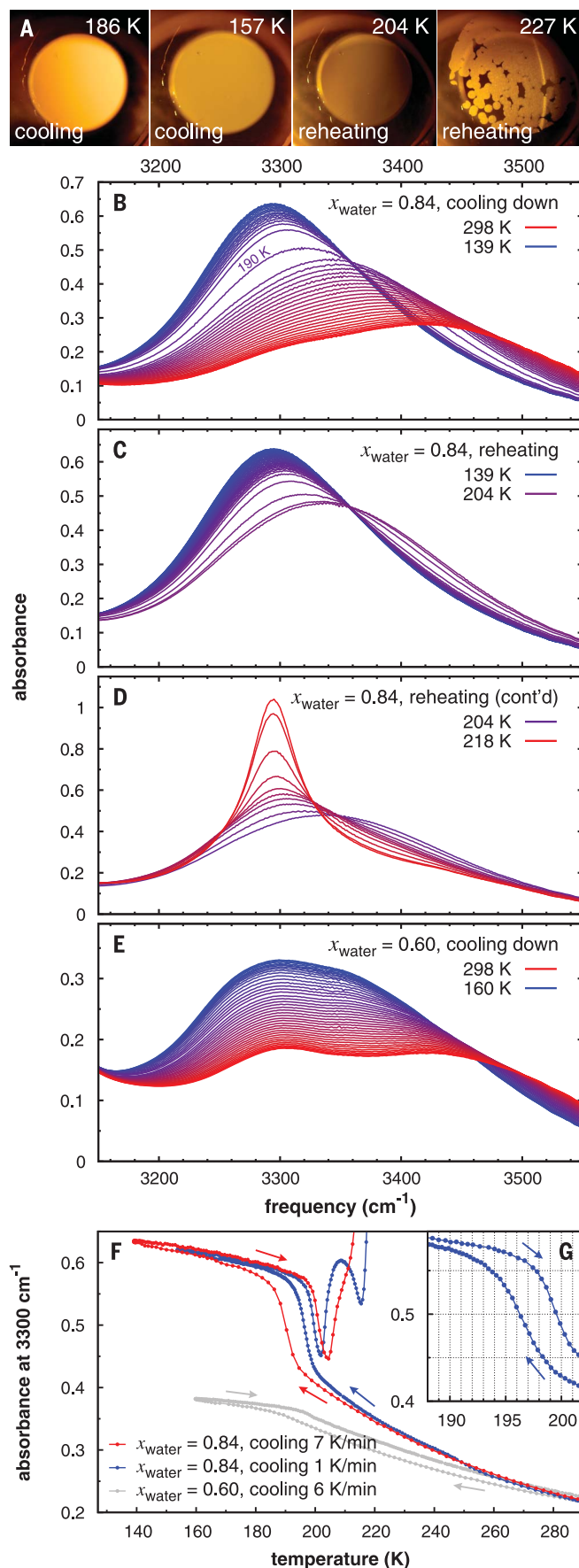
At 25°C, the OH/NH-stretch region contained a broad intense band centered at $3420 cm^{-1}$ and a much weaker peak at $3300 cm^{-1}$. The latter was absent from the spectrum of an NaTFA solution with the same x_{water} value (fig. S1) (16), which showed that the $3420 cm^{-1}$ peak arose from the OH-stretch mode of water (HDO), whereas the $3300 cm^{-1}$ peak arose from the NH-stretch mode of hydrazinium ($N_2HD_4^+$). This assignment was confirmed by the change in relative intensities of the two peaks upon changing the water fraction (Fig. 2E). The absorption spectrum of the fully deuterated solution showed negligible absorption in the investigated frequency region (fig. S4) (16). We attribute the striking jump in IR absorption observed in Fig. 2B in the lower temperature range (about 190 K) to the liquid-liquid transition, as discussed below.

The OH-stretch mode of the solution has a center frequency and width [245 cm^{-1} full width at half maximum (FWHM)] comparable to those of liquid HDO: D_2O (21), and in both cases the line shapes are approximately Gaussian. These similarities indicate that even at the high concentration of ions in the solution, the H-bond local structure surrounding a water molecule resembles that in neat water, as is reflected at the macroscopic level by the ideal-solution behavior already mentioned. Hydrazinium contains five H-bond-donating groups, and trifluoroacetate has five H-bond acceptor sites, so that N_2H_5TFA formed an H-bond network resembling that of water. This bonding motif has been shown previously for the similar ionic liquid ethyl ammonium nitrate (22). Thus, N_2H_5TFA fit remarkably well into the three-dimensional water H-bond network and left it essentially unperturbed, as was demonstrated by the OH-stretch spectrum consisting of a single absorption band at the same frequency as that of neat HDO: D_2O . The macroscopic ideal mixing behavior could thus be described as an ideal mixing of the structures.

This structural description was confirmed by molecular dynamics (MD) simulations of the

Fig. 2. Liquid-liquid transition in aqueous solution.

(A) Droplet of (N_2HD_4/N_2D_5)TFA solution in HDO/ D_2O (H/D fraction $\sim 3\%$) with $x_{water} = 0.84$, between two CaF_2 windows, during cooling and subsequent reheating. All temperatures given in the figures and text are those of a thermocouple close to the liquid layer (16). The circle is the optical exit of the sample holder. The circumference of the droplet is visible as the sharp squiggly line. During reheating, crystallization occurs (rightmost panel), but only after the liquid-liquid transition. (B) IR spectra of the same solution. Upon decreasing the temperature (at $7 K min^{-1}$), the OH-stretch peak showed a gradual redshift. At $\sim 190 K$, an intense, broad low-frequency OH-stretch mode appeared, indicating a discrete change in H-bond structure. (C) Upon reheating, this phenomenon was reversed and the low-frequency peak disappeared again. (D) Upon further reheating, the water crystallized, resulting in a narrow low-frequency OH-stretch peak (assigned to ice) superimposed on a broad OH/NH-stretch background caused by the surrounding liquid. (E) In a solution with a water fraction $x = 0.60$, no structural transition occurred, only a gradual lowering of the OH-stretch frequency with decreasing temperature. (F) IR absorbance at $3300 cm^{-1}$ versus temperature during cooling and reheating as indicated by the arrows. Each point indicates a measured IR spectrum. At a lower cooling and reheating rate, the hysteresis was much less. (G) Close-up showing the reduced hysteresis at a lower cooling rate.



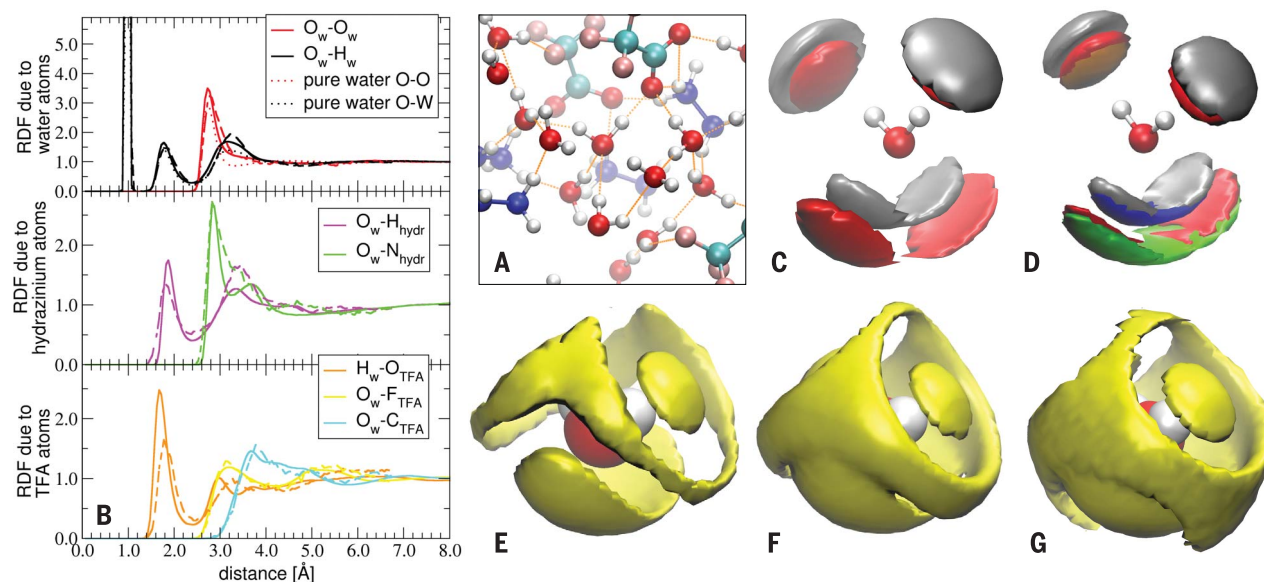


Fig. 3. MD simulations of the investigated solution. (A) Snapshot of the classical MD simulation. (B) Radial distribution functions (RDFs) of different H-bond donor and acceptor atoms in the solution around water atoms, obtained from the classical (solid lines) and DFT (dashed lines) MD simulations. In the top panel, radial distributions of the water O and H atoms are compared to these functions in bulk water (dotted lines). (C and D) Three-dimensional structural density plots of the first coordination shell of a water molecule, in neat water (C) and

in N_2H_5TFA solution (D), showing the distribution of different H-bond donor and acceptor atoms. Color code for isosurfaces: red, water O atom; gray, water H atom; orange, TFA O atom; blue, hydrazinium H atom; green, hydrazinium N atom. (E to G) Three-dimensional structural density plots of the H-bond acceptor atoms (water O, TFA O, and hydrazinium N) in the first and second coordination shells of a water molecule (in the center) in neat water at 1 bar (E), in neat water at 6 kbar (F), and in N_2H_5TFA solution at 1 bar (G).

N_2H_5TFA solution (Fig. 3). We performed both classical and ab initio simulations and found that the latter confirmed the former very well. The simulations showed that the ions fit well into the H-bond network of water (Fig. 3). The radial distribution functions (Fig. 3B) showed that in the first coordination shell of the water molecules in the solution, the H and N/O atoms of the solute partly replaced the water H and O atoms as H-bond donor and acceptor atoms. The N/O...H and N/O...O distance distributions in the solution were very similar to the O...H and O...O distributions in neat water. This similarity can be quantified by comparing the average H-bond coordination number of a water molecule in our ionic solution and in neat water, for which we found values of 4.3 and 3.8, respectively (table S1) (16).

Because H-bond directionality is an important structural characteristic of water, we also calculated the orientational distribution of the H-bond donor and acceptor atoms around water. These orientational distributions are again very similar in the solution and in neat water (Fig. 3, C and D): The hydrazinium H atoms partly replaced water H atoms as H-bond donors, and the hydrazinium N and TFA O atoms partly replaced water O atoms as H-bond acceptors (the spatial distributions of the H atoms of hydrazinium and water overlap so closely that the intersection of their isosurfaces in Fig. 3D is determined mostly by the noise in the simulations). The same holds for the hydrazinium N and water O atoms, and for the TFA O and water O atoms.

Finally, we investigated the second coordination shell of the water molecules. The structure of the solution (Fig. 3G) differed somewhat from that of neat water at ambient pressure (Fig. 3E). However, the second solvation shell structure of our solution is virtually identical to that of neat water at high pressure, which was determined previously from combined neutron-diffraction experiments and simulations (23, 24) and which we reproduced when performing a simulation of neat water at high pressure (6 kbar in Fig. 3F; intermediate pressures in fig. S8) (16). This similarity confirms the experiments by Leberman and Soper (25), demonstrating that adding salt modifies the water structure in the same way as increasing the pressure.

Upon cooling the solution (Fig. 2B), the frequency of the OH-stretch frequency initially decreased gradually, in a fashion similar to neat supercooled water (26). However, at a temperature close to that of the heat capacity spike (~ 190 K), a discontinuous change occurred: A new OH-stretch mode appeared at 3300 cm^{-1} and the initial OH-stretch mode vanished. Upon further cooling, this new OH-stretch mode also gradually decreased in frequency. The transition was reversible (Fig. 2C): Upon reheating the sample, the low-frequency OH-stretch mode disappeared and the original high-frequency OH-stretch mode reappeared.

The sample remained transparent during cooling, as well as during subsequent reheating to ~ 204 K. At that temperature, ice crystallites

started to form (Fig. 2A, rightmost panel). The presence of ice appeared distinctly in the IR spectrum (Fig. 2D) as a narrow peak at 3295 cm^{-1} with a width of 50 cm^{-1} . These numbers agreed well with the center frequency and width of the OH-stretch mode of HDO: D_2O ice at this temperature (27). The complete absence of the ice peak in the earlier stages of the temperature scan demonstrated that no ice formed during the structural transition associated with the heat capacity spike, neither during cooling nor during reheating. Crystallization occurred at a temperature above that of the heat capacity spike, and only during reheating, not during cooling. This is because crystallization requires both nucleation and growth, and the rate of the latter is generally much smaller than that of the former, which also peaks at a much lower temperature (27). Consequently, some nuclei (but no crystals) can be formed at the very lowest temperatures accessed during our experiment, but these nuclei can turn into crystals only at high temperatures (well above that of the heat capacity spike) where the growth rate is sufficient.

The discontinuous nature of the observed structural transition was visible when monitoring the absorbance at 3300 cm^{-1} during cooling and reheating (Fig. 2F). When cooling at a rate of 7 K min^{-1} (red points), the appearance (during cooling) and disappearance (during reheating) of the 3300 cm^{-1} peak occurred at temperatures that differed by about 10 K. However, when cooling at a rate of 1 K min^{-1} (blue points in Fig. 2F), the difference was only 3 K (28).

The discontinuous change in the OH-stretch spectrum indicated that the heat capacity spike involves an abrupt change in the H-bond structure. Thus, this transition cannot be a glass transition, which is an arrest—not a change—of structure (caused by the structural equilibration time scale becoming longer than the experimental time scale). The difference is well illustrated by a measurement on a sample with a water fraction of 0.60, which exhibited a glass transition, visible in differential scanning calorimetry as a step decrease in the heat capacity (like that seen in Fig. 1 for the LiCl solution, but at higher temperature). In the IR spectrum, however, we observed only a gradual shift and no discontinuity of the OH-stretch mode (Fig. 2E and gray points in Fig. 2F; note that the $x_{\text{water}} = 0.84$ and $x_{\text{water}} = 0.60$ data were obtained with the same cooling rate).

On the basis of the IR spectra, we can exclude the possibility that the heat capacity spike was caused by ice formation or by a glass transition. Rather, the observed change in H-bond structure indicates that the heat capacity spike can be associated with a phase transition involving a change in the H-bond structure. The OH-stretch spectrum provided direct information on the differences in H-bond structures between the high-temperature and low-temperature liquid phases (Fig. 4): The lower center frequency implies stronger (shorter) H bonds in the low-temperature liquid (relative to the high-temperature liquid), whereas the smaller width ($\sim 180 \text{ cm}^{-1}$ FWHM) indicates that the H-bond structure is more ordered.

The spectral changes (redshift, narrowing, asymmetry) during the transition from the high- to the low-temperature phase were similar to the changes when going from low-density amorphous (LDA) to high-density amorphous (HDA) water (29–31) (Fig. 4). The spectra of our solutions have somewhat larger widths, indicating more disorder, probably because of the presence of the ions. The similarity of these spectra strongly suggests that the liquid-liquid transition observed here is directly connected to the HDA-LDA transition in water. The equivalence of high ionic concentrations with the application of high pressure (22), as confirmed by our simulations, strongly suggests that a liquid-liquid transition also exists in neat water, as was predicted by Poole (1) and others (32) and indicated by recent evaporative cooling experiments (33, 34). We hope that our studies will stimulate further work to confirm this implication—for instance, by studying the effect of pressure (by increasing the pressure in the low-temperature phase, it should be possible to recross the liquid-liquid phase line), ionic concentration, and isotope composition [to investigate the role of nuclear quantum effects (34)].

A solid theoretical basis for this scenario has been provided by the groups of Anisimov (7) and Debenedetti (5), who have shown that a liquid-liquid transition in a binary mixture

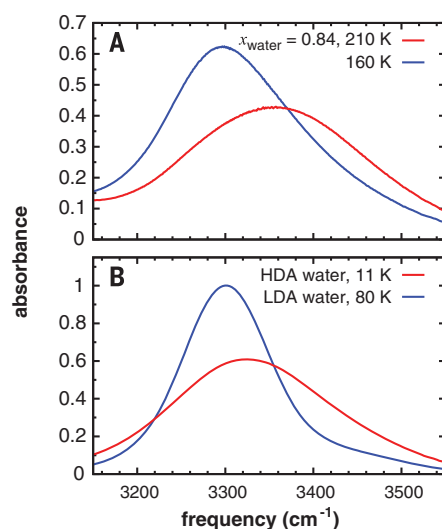


Fig. 4. IR absorption spectra of the two liquid phases and amorphous water. (A) High-temperature and low-temperature liquid phases observed in our experiment. (B) Low-density and (vapor-deposited) high-density amorphous water; data were measured as described in (30, 31) and provided by the authors of those papers. In (B), the LDA spectrum was normalized to its maximum, and the HDA spectrum was normalized so as to have the same frequency-integrated absorption as the LDA spectrum.

need not require the usual nonideal positive heat of mixing in the binary solution but can arise purely as a consequence of an anomalous tendency to liquid-liquid unmixing (i.e., polymorphism) in the pure solvent. The liquid-liquid transition we observed in our crystallization-resistant aqueous solution has all of the features predicted for the latter source of first-order solution transition and would seem to provide direct evidence for the existence of a liquid-liquid transition behind the “crystallization curtain” in pure water. Our IR measurements and MD simulations both indicate that the structures of the two liquid phases are very similar to those of the liquid phases to be expected in neat water at high pressure; thus, they provide forceful arguments for the occurrence of a liquid-liquid transition (similar to the one observed here) in neat water at elevated pressure. In this case, our findings would provide a unifying explanation for the thermodynamic anomalies of liquid water.

REFERENCES AND NOTES

1. P. H. Poole, F. Sciortino, U. Essmann, H. E. Stanley, *Nature* **360**, 324–328 (1992).
2. P. H. Poole, F. Sciortino, T. Grande, H. E. Stanley, C. A. Angell, *Phys. Rev. Lett.* **73**, 1632–1635 (1994).
3. M. G. Sceats, S. A. Rice, in *Water: A Comprehensive Treatise*, F. Franks, Ed. (Plenum, 1982), vol. 7, pp. 83–211.
4. H. Kanno, C. A. Angell, *J. Chem. Phys.* **70**, 4008–4016 (1979).
5. S. Chatterjee, P. G. Debenedetti, *J. Chem. Phys.* **124**, 154503 (2006).

6. M. A. Anisimov, *Russ. J. Phys. Chem. B* **6**, 861–867 (2012).
7. J. W. Biddle, V. Holten, M. A. Anisimov, *J. Chem. Phys.* **141**, 074504 (2014).
8. D. G. Archer, R. W. Carter, *J. Phys. Chem. B* **104**, 8563–8584 (2000).
9. C. A. Angell, *Science* **319**, 582–587 (2008).
10. J. Riemenschneider, R. Ludwig, *J. Chem. Phys.* **135**, 117101 (2011).
11. M. Oguni, C. A. Angell, *J. Chem. Phys.* **73**, 1948–1954 (1980).
12. Z. Zhao, C. A. Angell, *Angew. Chem. Int. Ed.* **55**, 2474–2477 (2016).
13. W. J. Moore, *Physical Chemistry* (Prentice-Hall, ed. 4, 1972).
14. D. Corradini, M. Rovere, P. Gallo, *J. Chem. Phys.* **132**, 134508 (2010).
15. D. Corradini, M. Rovere, P. Gallo, *J. Phys. Chem. B* **115**, 1461–1468 (2011).
16. See supplementary materials.
17. K. Murata, H. Tanaka, *Nat. Mater.* **11**, 436–443 (2012).
18. M. Yang, J. L. Skinner, *Phys. Chem. Chem. Phys.* **12**, 982–991 (2010).
19. A. K. Wyczkowska, K. S. Abdulkadirova, M. A. Anisimov, J. V. Sengers, *J. Chem. Phys.* **113**, 4985–5002 (2000).
20. C. A. Angell, E. J. Sare, J. Donnelly, D. R. MacFarlane, *J. Phys. Chem.* **85**, 1461–1464 (1981).
21. T. A. Ford, M. Falk, *Can. J. Chem.* **46**, 3579–3586 (1968).
22. K. Fumino, A. Wulf, R. Ludwig, *Angew. Chem. Int. Ed.* **48**, 3184–3186 (2009).
23. P. G. Debenedetti, H. E. Stanley, *Phys. Today* **56**, 40–46 (2003).
24. A. K. Soper, M. A. Ricci, *Phys. Rev. Lett.* **84**, 2881–2884 (2000).
25. R. Leberman, A. K. Soper, *Nature* **378**, 364–366 (1995).
26. F. Perakis, P. Hamm, *J. Phys. Chem. B* **115**, 5289–5293 (2011).
27. H. Senapati, K. K. Kadiyala, C. A. Angell, *J. Phys. Chem.* **95**, 7050–7054 (1991).
28. This small difference probably originated mainly from the sample temperature lagging behind the temperature of the thermocouple (see fig. S3), which was not immersed in the liquid but attached to the brass holder keeping the CaF₂ windows together.
29. O. Mishima, Y. Suzuki, *Nature* **419**, 599–603 (2002).
30. A. Shalit, F. Perakis, P. Hamm, *J. Phys. Chem. B* **117**, 15512–15518 (2013).
31. A. Shalit, F. Perakis, P. Hamm, *J. Chem. Phys.* **140**, 151102 (2014).
32. P. Gallo *et al.*, *Chem. Rev.* **116**, 7463–7500 (2016).
33. P. Gallo, H. E. Stanley, *Science* **358**, 1543–1544 (2017).
34. K. H. Kim *et al.*, *Science* **358**, 1589–1593 (2017).

ACKNOWLEDGMENTS

We thank H. Sanders for preparing the samples and A. Shalit and P. Hamm for providing the data shown in Fig. 4B. **Funding:** Supported by the John van Geuns Foundation (S.W.) and NSF grant CHE 12-13265 (C.A.A.). **Author contributions:** C.A.A. and S.W. conceived the experiments; Z.Z. and C.A.A. performed and analyzed the calorimetric measurements; M.H. and S.W. performed and analyzed the cryogenic IR measurements; B.E. performed and analyzed the MD simulations; and C.A.A., S.W., and B.E. jointly wrote the manuscript. **Competing interests:** None declared. **Data and materials availability:** All data are reported in the main text and supplement and are also publicly available at the University of Amsterdam’s Figshare (doi: 10.21942/uva.5808366).

SUPPLEMENTARY MATERIALS

www.sciencemag.org/content/359/6380/1127/suppl/DC1
Materials and Methods
Supplementary Text
Figs. S1 to S8
Table S1
References (35–44)

27 September 2017; accepted 24 January 2018
10.1126/science.aao7049